PNAS
www.pnas.org

Supplementary Information for

Broadband lightweight flat lenses for longwave-infrared imaging

Monjurul Meem, Sourangsu Banerji, Apratim Majumder, Fernando Guevara Vasquez, Berardi Sensale-Rodriguez, Rajesh Menon

Rajesh Menon
Email: rmenon@eng.utah.edu

This PDF file includes:

www.pnas.org/cgi/doi/10.1073/pnas.1908447116

1. Dispersion of AZ9260 and Si in LWIR band

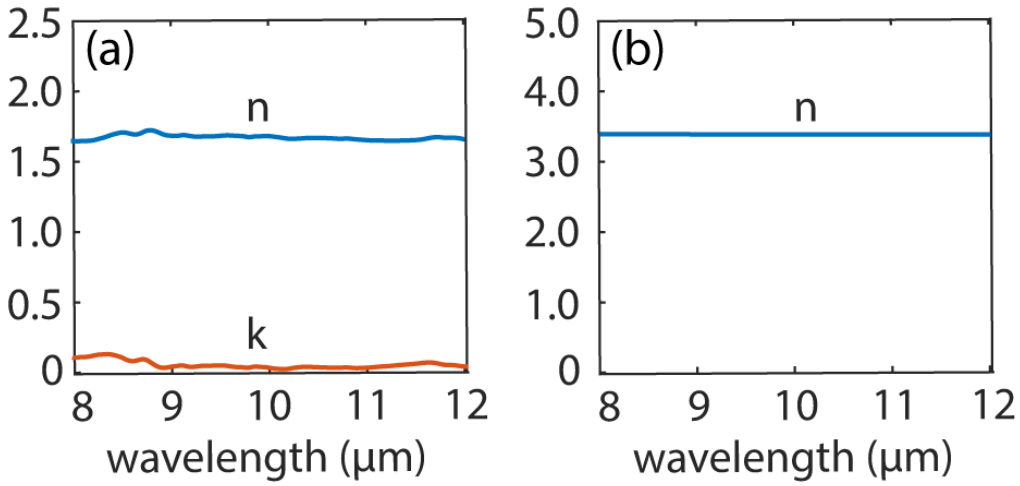

Fig. S1: *Dispersion of (a) AZ9260 and (b) Silicon in the LWIR band.*

2. Focusing Efficiency Spectra of the 2 lenses in Fig. 1.

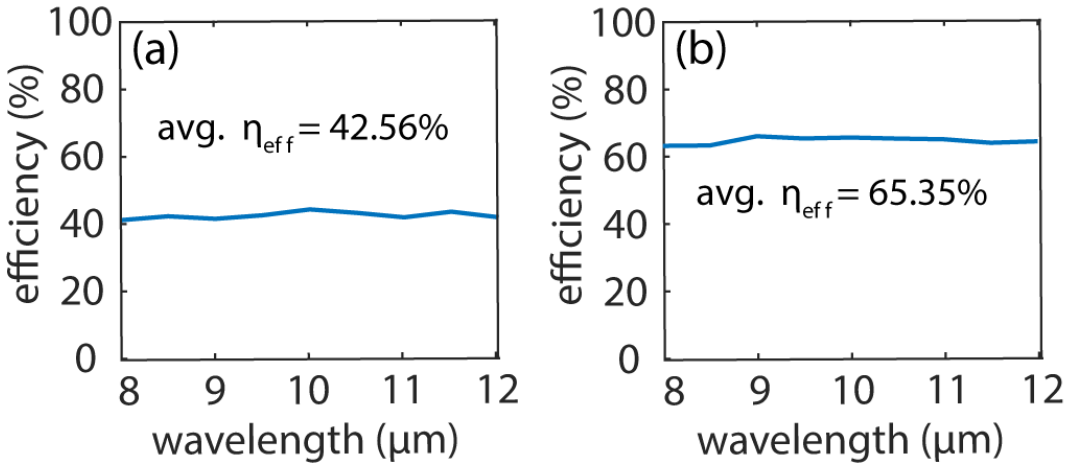

Fig. S2 : *Focusing efficiency spectra of lens with (a) f=19mm, NA=0.371 and (b) f=8mm, NA=0.45. Both designs are shown in Fig. 1 of the main text.*

3. Full-Width at Half-Maximum of the Focal Spots of the 2 lenses in Fig. 1.

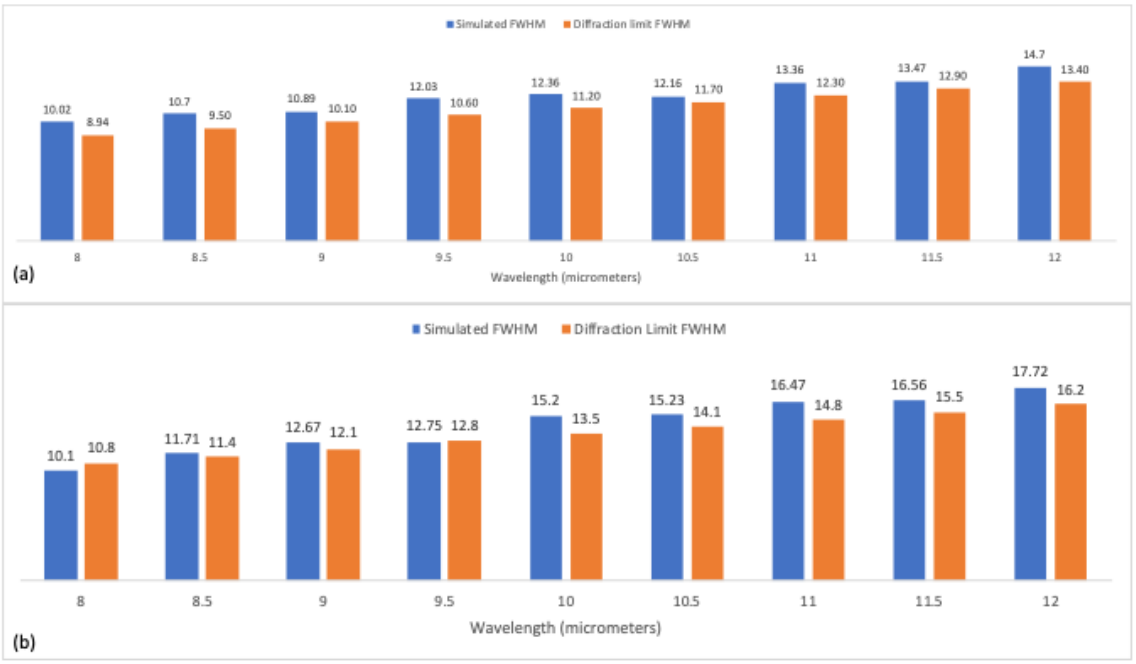

Fig. S3: *Simulated full-width at half-maximum (FWHM) of the focal spots (shown in blue) of lens with (a) f=19mm, NA=0.371 and (b) f=8mm, NA=0.45. The corresponding diffraction limited FWHM are shown in orange for comparison. Both designs are shown in Fig. 1 of the main text.*

4. Absorption in Polymer Film of the 2 lenses in Fig. 1.

The absorption in the film was computed using the extinction coefficient, $\alpha = 4\pi k/\lambda$, where k is the complex part of the measured refractive index. The absorbed fraction is then computed as $1 - \exp(-\alpha * h)$, where h is the ring height of each ring in the lens. We can then average the absorption across all the rings to compute an estimate of the total absorption.

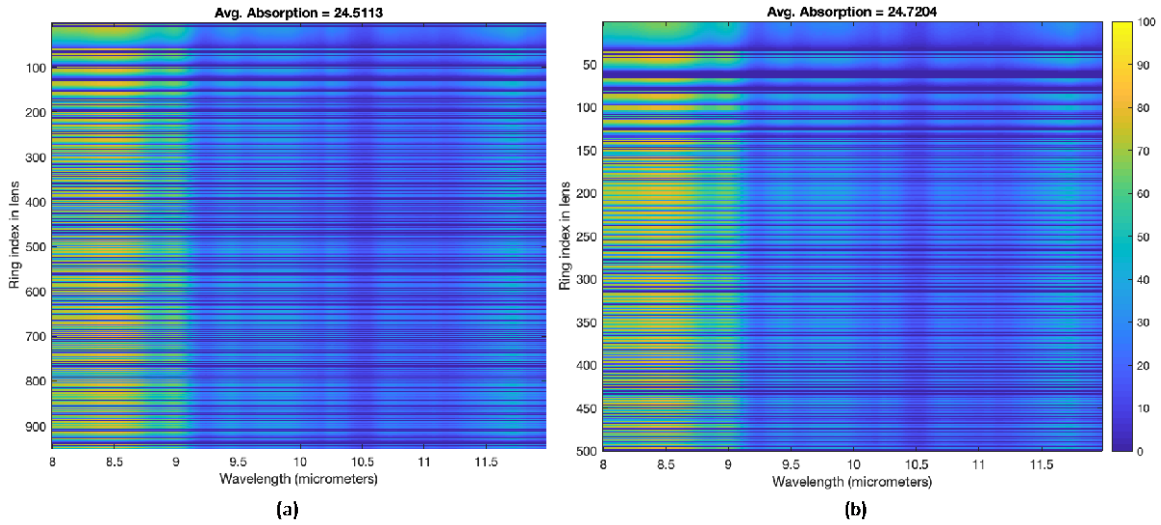

Fig. S4: *Calculated absorption in the AZ9260 film as function of wavelength and ring index for lens with (a) f=19mm, NA=0.371 and (b) f=8mm, NA=0.45. The absorption averaged over the entire lens is shown on top for each lens. Both designs are shown in Fig. 1 of the main text.*

5. Aberrations Analysis

The Zernike polynomial coefficient were fitted over a circular shaped pupil. The fit was using the least squares fit method. Fringe indexing scheme was used.

Table S1: Aberrations coefficients

Radial degree (n)	Azimuthal degree (m)	Fringe index (j)	Classical name
0	0	1	piston
1	1	2	tip
1	-1	3	tilt
2	0	4	defocus
2	2	5	vertical astigmatism
2	-2	6	oblique astigmatism
3	1	7	horizontal coma
3	-1	8	vertical coma
4	0	9	primary spherical
3	3	10	oblique trefoil
3	-3	11	vertical trefoil
4	2	12	vertical secondary astigmatism
4	-2	13	oblique secondary astigmatism
4	4	14	vertical quadrafoil
4	-4	15	oblique quadrafoil

The following lists all the fitting coefficients for the designed lenses:

Table S2: Flat Lens with NA = 0.371, f = 19 mm

Wavelength (um)	Piston	Tip	Tilt	Defocus	Vertical astigmatism	Oblique astigmatism	Horizontal coma	Vertical coma	Primary spherical	Oblique trefoil	Vertical trefoil	Vertical secondary astigmatism	Oblique secondary astigmatism	Vertical quadrafoil	Oblique quadrafoil
8	2.42E-05	-1.14E-08	-1.14E-08	-4.50E-05	-2.01E-21	1.13E-11	2.49E-08	2.49E-08	3.50E-05	1.09E-09	-1.09E-09	-1.55E-20	3.41E-11	-6.17E-06	-5.46E-23
8.5	2.04E-05	-9.01E-09	-9.01E-09	-3.79E-05	1.93E-21	-2.34E-11	1.98E-08	1.98E-08	3.09E-05	1.14E-09	-1.14E-09	-6.88E-22	-2.79E-11	-5.14E-06	7.36E-23
9	2.02E-05	-4.36E-09	-4.36E-09	-3.98E-05	-7.17E-22	-1.55E-11	5.80E-09	5.80E-09	3.93E-05	6.73E-10	-6.73E-10	-2.55E-20	-2.58E-11	-3.95E-06	-1.15E-23
9.5	2.23E-05	-5.33E-09	-5.33E-09	-4.30E-05	-3.01E-21	2.56E-11	7.94E-09	7.94E-09	4.14E-05	1.50E-09	-1.50E-09	-1.67E-21	4.28E-11	-4.51E-06	4.55E-23

10	1.89E-05	-4.99E-09	-4.99E-09	-3.63E-05	1.07E-20	-1.83E-11	3.19E-09	3.19E-09	3.56E-05	-1.33E-09	1.33E-09	-1.80E-21	-3.04E-11	-3.57E-06	-8.18E-23
10.5	2.01E-05	-3.98E-09	-3.98E-09	-3.78E-05	7.35E-22	-1.41E-11	5.42E-09	5.42E-09	3.61E-05	3.43E-11	-3.43E-11	-6.83E-21	-2.41E-11	-3.82E-06	-1.95E-23
11	2.57E-05	-5.09E-09	-5.09E-09	-4.76E-05	5.49E-21	1.34E-10	6.59E-09	6.59E-09	4.38E-05	8.18E-10	-8.18E-10	-6.53E-21	2.22E-10	-4.82E-06	-2.14E-23
11.5	2.41E-05	-5.53E-09	-5.53E-09	-4.32E-05	-1.12E-20	1.29E-11	1.18E-08	1.18E-08	3.67E-05	1.97E-09	-1.97E-09	-1.68E-20	-2.39E-11	-5.04E-06	1.03E-22
12	1.77E-05	-3.62E-09	-3.62E-09	-3.17E-05	2.54E-21	-7.91E-12	7.00E-09	7.00E-09	2.72E-05	1.13E-09	-1.13E-09	7.39E-21	-1.17E-11	-3.54E-06	-2.11E-23

Table S3: Flat Lens with NA = 0.45, f = 8 mm

Wavelength (um)	Piston	Tip	Tilt	Defocus	Vertical astigmatism	Oblique astigmatism	Horizontal coma	Vertical coma	Primary spherical	Obliqueue trefoil	Vertical trefoil	Vertical secondary astigmatism	Oblique secondary astigmatism	Vertical quadrafoil	Oblique quadrafoil
8	1.08E-05	-5.77E-09	-5.77E-09	-2.66E-05	2.71E-21	-3.38E-12	1.70E-08	1.70E-08	3.10E-05	-7.64E-10	7.64E-10	-2.00E-21	7.98E-12	-3.74E-07	-5.61E-24
8.5	9.09E-06	-4.71E-09	-4.71E-09	-2.22E-05	-2.62E-21	-3.54E-12	1.36E-08	1.36E-08	2.61E-05	-7.66E-10	7.66E-10	1.87E-21	5.07E-12	-2.68E-07	9.79E-24
9	9.00E-06	-2.23E-09	-2.23E-09	-2.23E-05	-8.18E-22	-1.47E-12	6.37E-09	6.37E-09	2.77E-05	-3.68E-10	3.68E-10	-5.04E-22	1.98E-12	-1.46E-07	-2.04E-24
9.5	1.00E-05	-2.87E-09	-2.87E-09	-2.47E-05	1.10E-21	5.52E-13	7.18E-09	7.18E-09	3.02E-05	-7.48E-10	7.48E-10	-1.45E-22	5.82E-12	-2.08E-07	-4.30E-25
10	8.53E-06	-1.72E-09	-1.72E-09	-2.09E-05	-5.65E-22	-3.43E-12	4.83E-09	4.83E-09	2.55E-05	-3.08E-10	3.08E-10	6.60E-21	-3.12E-12	-2.20E-07	-1.41E-23
10.5	9.06E-06	-1.53E-09	-1.53E-09	-2.19E-05	1.41E-23	2.39E-12	5.02E-09	5.02E-09	2.65E-05	-5.63E-11	5.63E-11	7.55E-21	6.04E-12	-2.88E-07	3.20E-24
11	1.16E-05	-1.71E-09	-1.71E-09	-2.78E-05	2.06E-21	2.74E-12	6.24E-09	6.24E-09	3.32E-05	1.78E-10	-1.78E-10	3.43E-21	6.53E-12	-3.75E-07	-2.53E-24
11.5	1.08E-05	-2.15E-09	-2.15E-09	-2.56E-05	-1.23E-21	6.82E-13	8.51E-09	8.51E-09	2.99E-05	2.79E-10	-2.79E-10	-5.00E-21	5.27E-12	-3.98E-07	-9.79E-24
12	7.97E-06	-1.09E-09	-1.09E-09	-1.88E-05	-3.36E-21	1.82E-12	4.46E-09	4.46E-09	2.20E-05	1.77E-10	-1.77E-10	4.37E-22	4.02E-12	-2.63E-07	-7.94E-25

6. Fabrication

The MDLs were fabricated using direct laser write grayscale lithography [1]. Previously we have demonstrated grayscale lithography with positive thin photoresist [2], this time used a thick photoresist, as we needed taller pixels for LWIR lens. A positive tone photoresist (AZ9260) [3] was spin coated on a 1" double sided polished Si wafer at 2000 rpm for 60 seconds to yield a thickness of 10µm. The spin-coated sample was baked in an oven at 110°C for 30 minutes. The samples were then left overnight inside a rehydration chamber (RH~60%). The designs were written on the sample using a Heidelberg µPG 101 [4] tool and developed in AZ 300 MIF developer [5] solution for 15 minutes. A calibration step was performed beforehand to determine the exposed depths at a particular gray scale level. The nonlinear relationship between the exposed depth and grayscale level depends on a given set of process variables - i.e. photoresist type, photoresist thickness, hard/soft baking time, humidity, developer used, developing time, Heidelberg µPF 101 settings and so on. A new calibration has to be done whenever there is a change in any aspect of the photoresist processing. The tool we used allows 100 different grayscale levels. The exposed depth profile vs grayscale level for a particular calibration is given fig. S5.

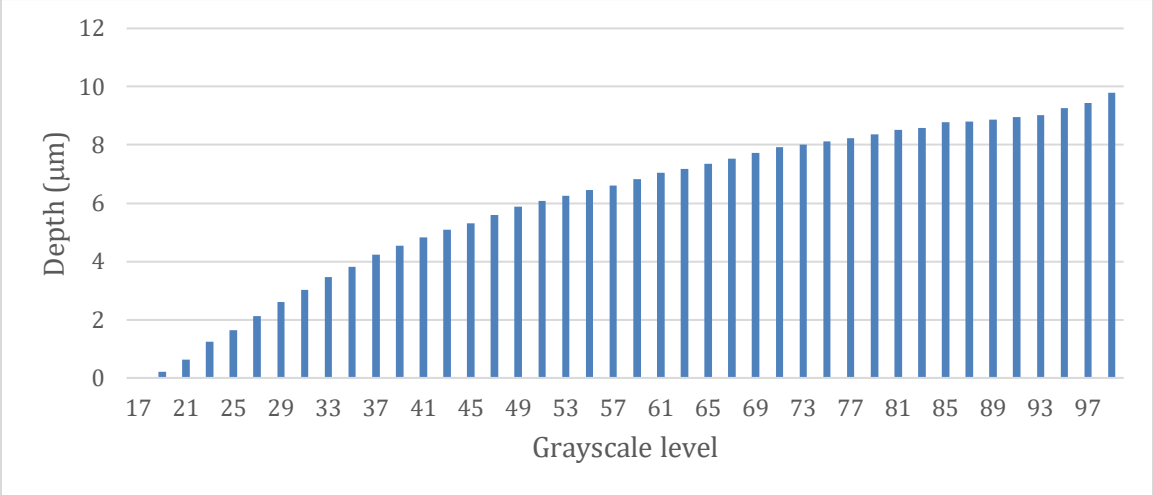

Fig. S5: *Exposed depth vs grayscale level*

7. Metrology of the fabricated lens

We measured the heights of the fabricated design (f=19mm, NA=0.371) over 10 randomly selected rings using a stylus profilometer (Tencor P-10). The results are summarized in fig. S6. The estimated error has a mean of 1.28μm and standard deviation of 800nm.

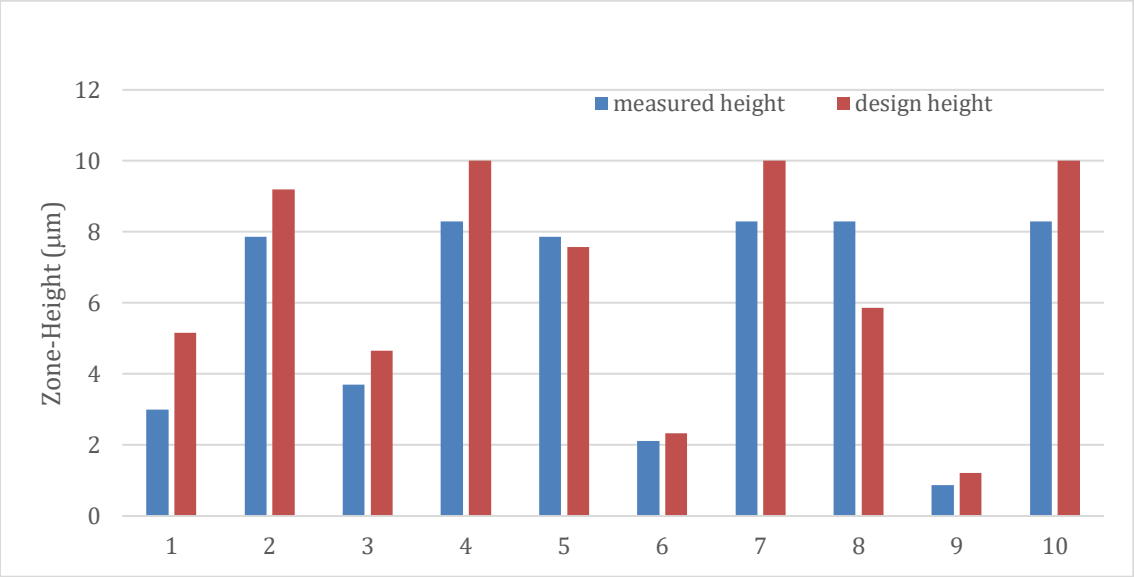

Fig. S6: *Ring-height measurement.*

8. Experiment Details

For imaging experiments, the LWIR lens was mounted on a xyz translation stage. Different hot objects were imaged onto a thermal sensor. We used two different thermal sensors; Tau 2 336 thermal core (FLIR) and LW-AAA thermal sensor (SeekThermal). The experimental setup is demonstrated in fig. S7.

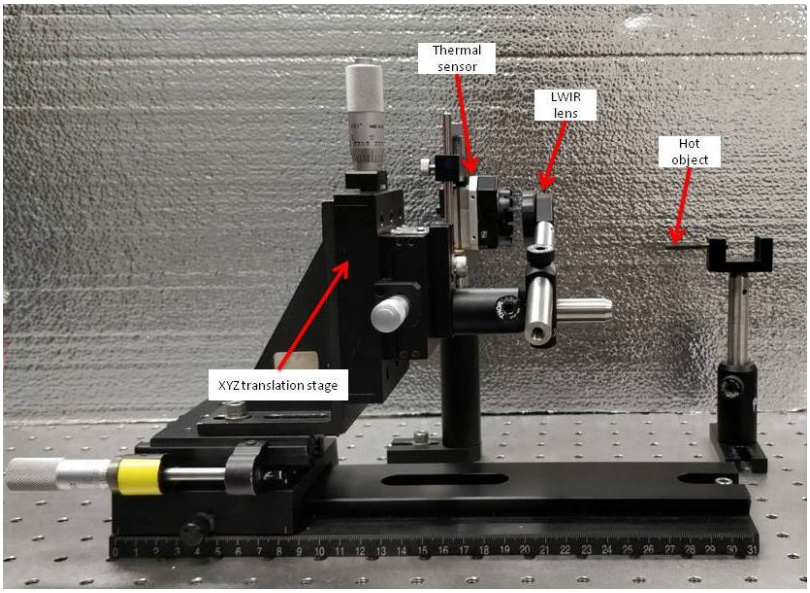

Fig. S7: *Experimental setup for imaging.*

For Imaging, different items were used as object and imaged onto the thermal sensor using LWIR lens. Some of the objects are presented in fig. S8.

For MTF calculation we imaged the slanted edge of an insulator (Plexiglas + Styrofoam) with a hotplate (Model: HS 30, Torrey Pines Scientific) behind it, as shown in fig. S8 (b). The temperature of the hotplate was varied from 60°C to 160°C. For all slanted edge images at different temperature, the object distance and image distance were kept fixed at 508mm and 20mm respectively. In each case, an image of the background with no heat source in front was taken, which served as dark frame and was subtracted from the images.

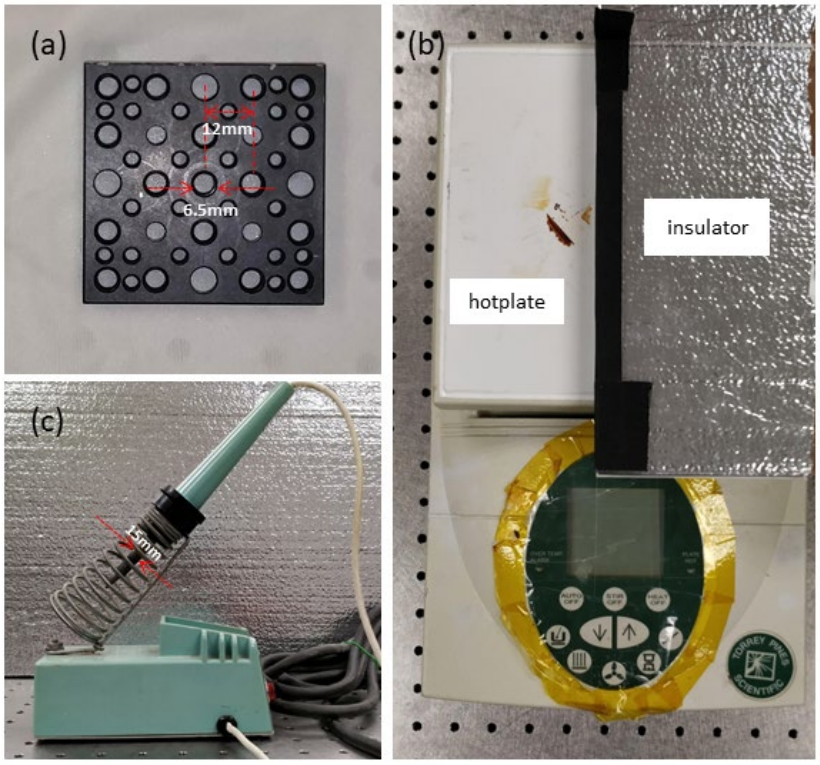

Fig. S8: *Objects used for imaging. (a) metal block with holes, used in main fig.5 (e) - (i), (b) hotplate with insulator in front, used for MTF characterization, (c) soldering iron, used for fig. 5(c)*

For efficiency measurement, we imaged a nail (diameter = 4.5mm) as an object (shown in fig. S8). The nail was heated to the desired temperature with a torch and then was imaged onto the Tau2 thermal sensor. A dark frame was also captured using aforementioned technique and subtracted from the images as well. The efficiency was estimated using the formula, efficiency = sum of pixel values in 3*W / sum of pixel values in full frame. The PSFs and W used for the efficiency measurements are given in fig. S9 and fig. S10 respectively.

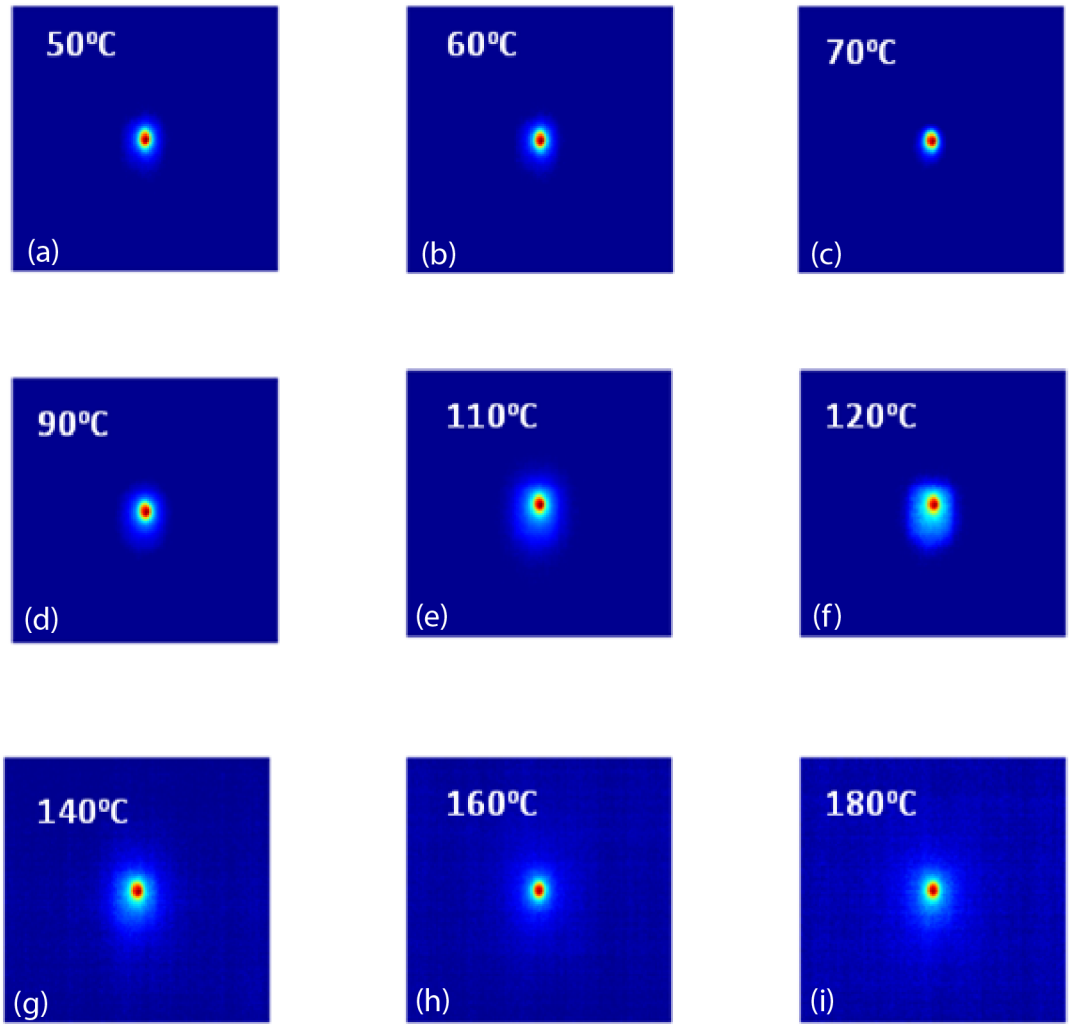

Fig. S9: *PSF's at different temperatures: (a) 50˚C (b) 60˚C (c) 70˚C (d) 90˚C (e) 110˚C (f) 120˚C (g) 140˚C (h) 160˚C and (i) 180˚C*

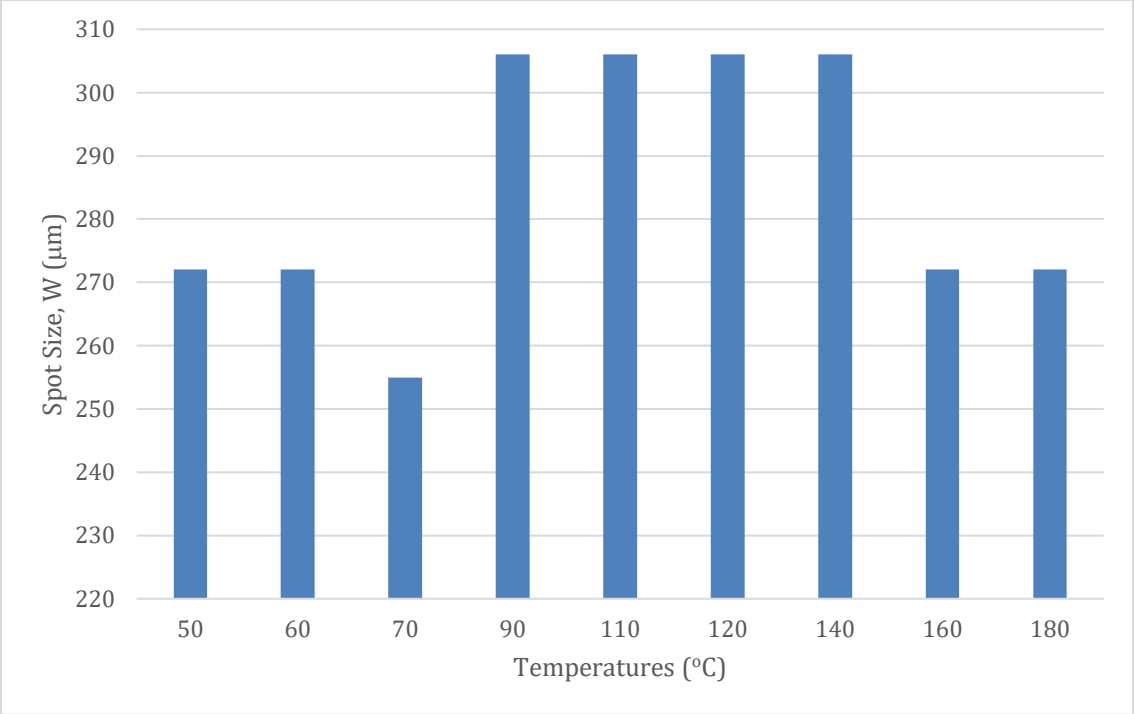

Fig. S10: *Spot size (W) at different temperatures.*

9. Camera Assembly

We put the LWIR lens on a 3D printed lens mount and attached it directly to Tau2 thermal sensor to make a standalone thermal camera. The demo camera is illustrated in fig S11. The lens mount can be adjusted for better focusing as well.

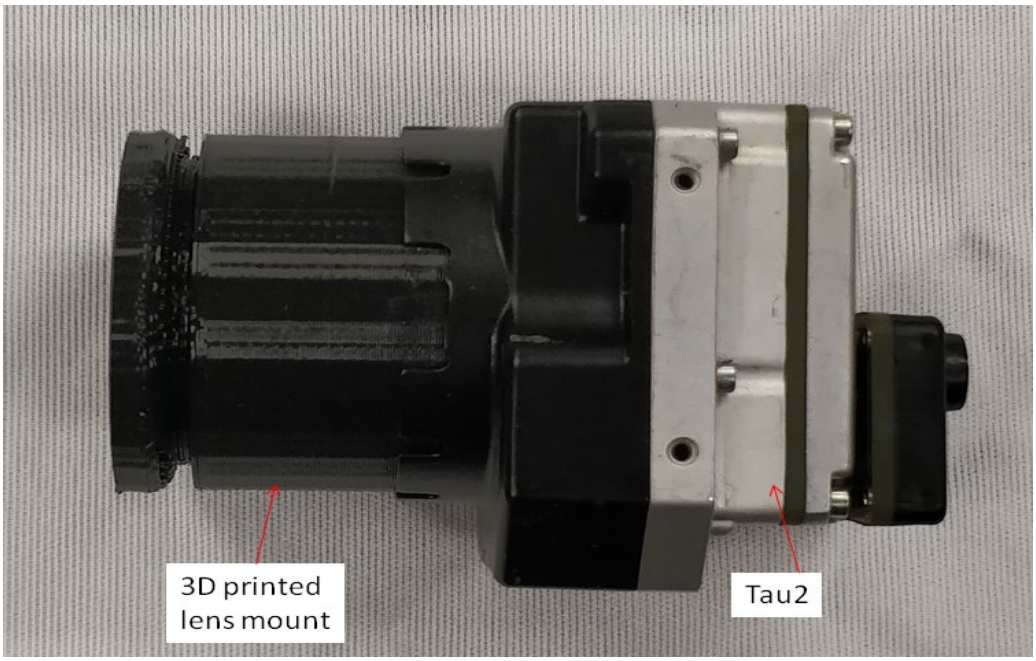

Fig. S11: *Demo camera assembly*

10. Simulated Point Spread Functions (PSFs) [Si Flat Lenses]

The simulated point spread functions (PSFs) for the broadband lenses designed with 8, 16, 32 and 64 height-quantized levels are provided below:

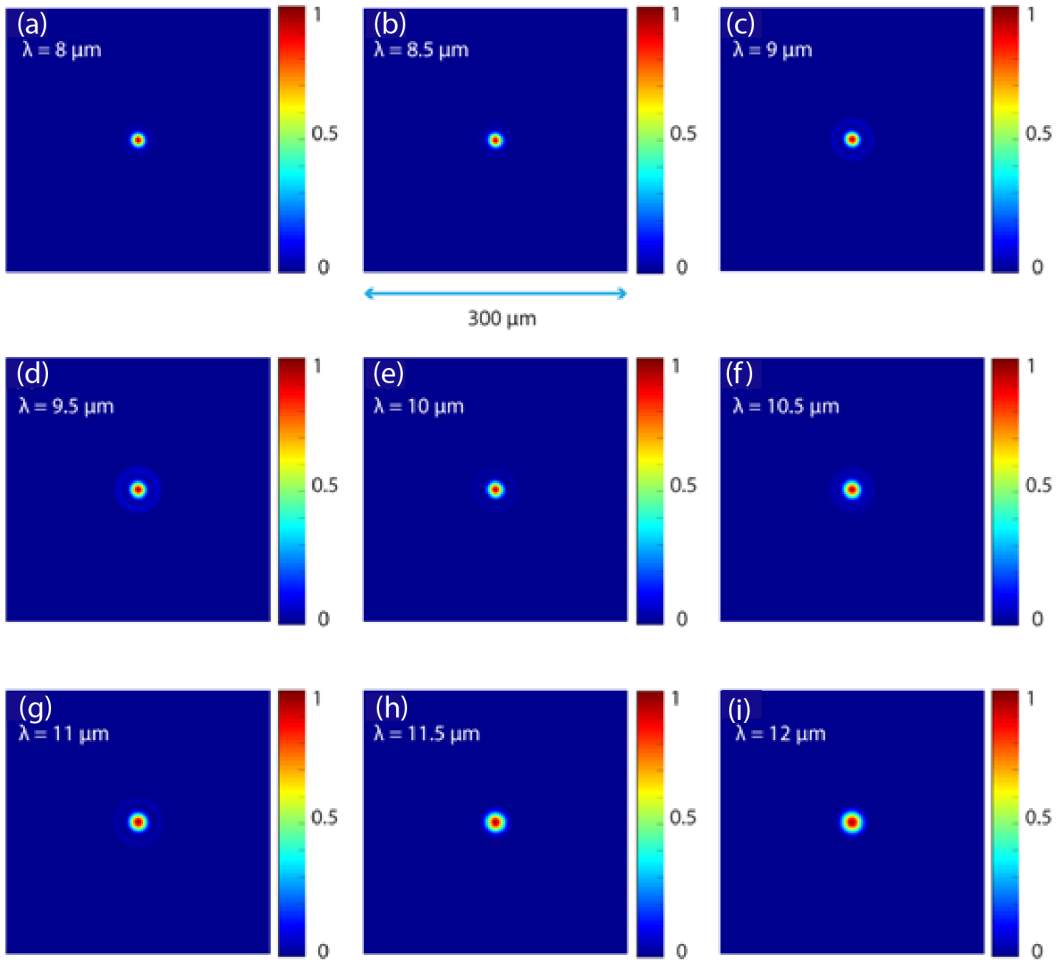

Fig. S12: *Simulated PSFs of the 8-level Si lens : (a) 8 μm (b) 8.5 μm (c) 9 μm (d) 9.5 μm (e) 10 μm (f) 10.5 μm (g) 11 μm (h) 11.5 μm and (i) 12 μm*

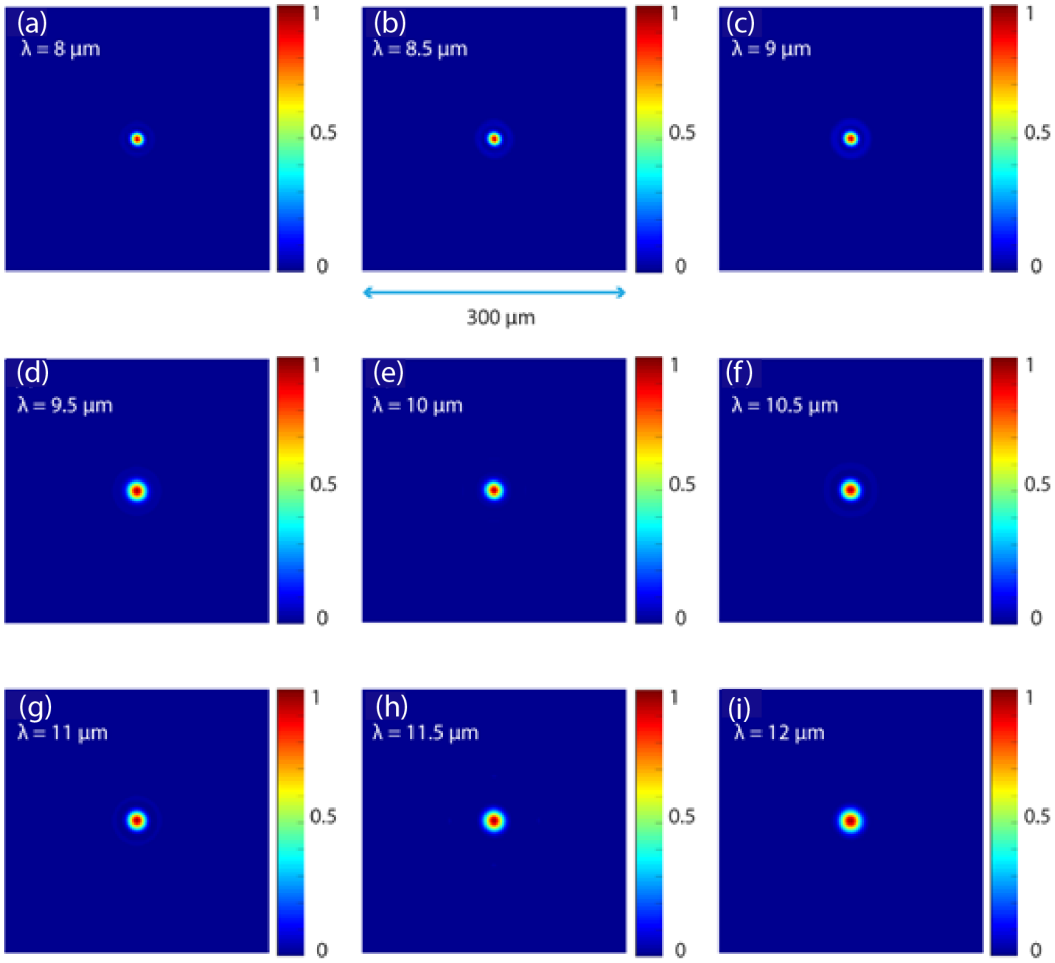

Fig. S13: *Simulated PSFs of the 16-level Si lens : (a) 8 μm (b) 8.5 μm (c) 9 μm (d) 9.5 μm (e) 10 μm (f) 10.5 μm (g) 11 μm (h) 11.5 μm and (i) 12 μm*

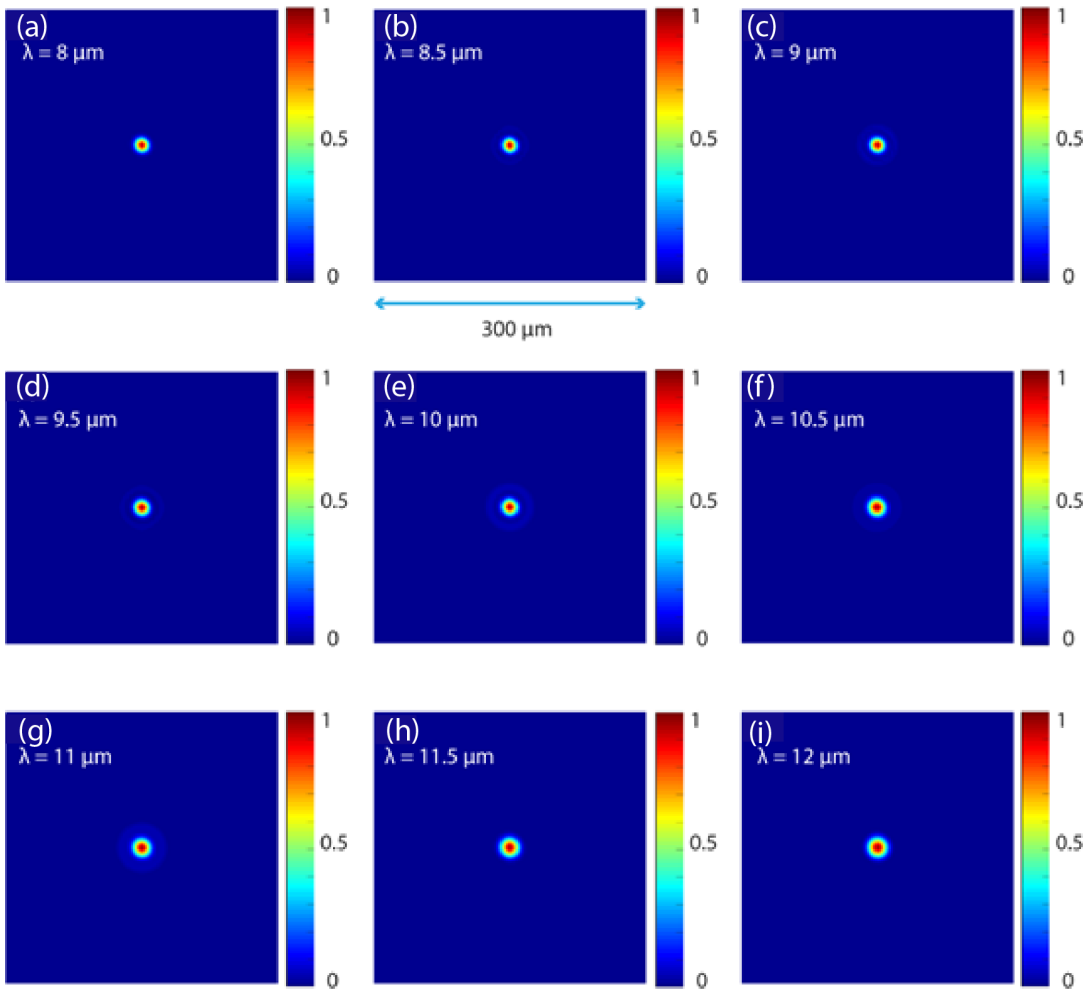

Fig. S14: *Simulated PSFs of the 32-level Si lens : (a) 8 μm (b) 8.5 μm (c) 9 μm (d) 9.5 μm (e) 10 μm (f) 10.5 μm (g) 11 μm (h) 11.5 μm and (i) 12 μm*

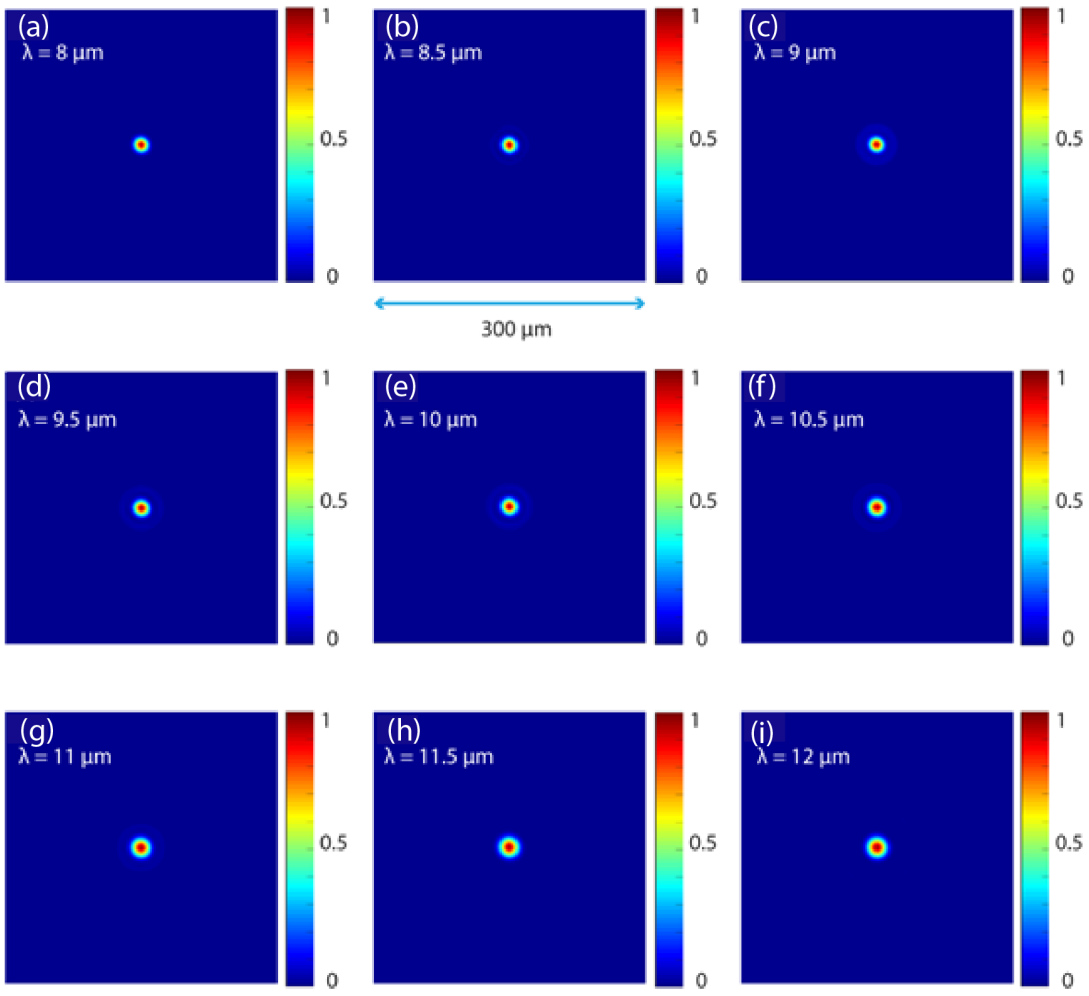

Fig. S15: *Simulated PSFs of the 64-level Si lens : (a) 8 µm (b) 8.5 µm (c) 9 µm (d) 9.5 µm (e) 10 µm (f) 10.5 µm (g) 11 µm (h) 11.5 µm and (i) 12 µm*

Supplementary Movies

Movie S1 (separate file): *Video1_SeekThermal_NA_045_f_8mm*

Movie S2 (separate file): *Video2_Tau2_NA0.371_f19mm_resistor*

Movie S3 (separate file): *Video3_Tau2_NA0.371_f19mm_indoor_human*

Movie S4 (separate file): *Video4_Tau2_NA0.371_f19mm_outdoor_human*

References

[1] McKenna, Curt, Kevin Walsh, Mark Crain, and Joseph Lake. "Maskless Direct Write Grayscale Lithography for MEMS Applications." In *Micro/Nano Symposium (UGIM), 2010 18th Biennial University/Government/Industry*, pp. 1-4. IEEE, 2010.

[2] Wang, Peng, Jose A. Dominguez-Caballero, Daniel J. Friedman, and Rajesh Menon. "A new class of multi-bandgap high-efficiency photovoltaics enabled by broadband diffractive optics." *Progress in Photovoltaics: Research and Applications* 23, no. 9 (2015): 1073-1079.

[3] Data sheet of AZ 9260 photoresist:

https://www.microchemicals.com/micro/az_9200.pdf

[4] Data sheet of Heidelberg μPG 101:

http://www.himt.de/index.php/upg-101.html

[5] Data sheet of AZ 300MIF developer:

http://www.imicromaterials.com/index.php/Products/Developers/mif-specs